# Implementation of Dynamical Nucleation Theory Effective Fragment Potentials Method for Modeling Aerosol Chemistry

Ajitha Devarajan, Theresa L. Windus, and Mark S. Gordon*

Department of Chemistry and Ames Laboratory, Iowa State University, Ames, Iowa 50011, United States

ABSTRACT: In this work, the dynamical nucleation theory (DNT) model using the ab initio based effective fragment potential (EFP) is implemented for evaluating the evaporation rate constant and molecular properties of molecular clusters. Predicting the nucleation rates of aerosol particles in different chemical environments is a key step toward understanding the dynamics of complex aerosol chemistry. Therefore, molecular scale models of nanoclusters are required to understand the macroscopic nucleation process. On the basis of variational transition state theory, DNT provides an efficient approach to predict nucleation kinetics. While most DNT Monte Carlo simulations use analytic potentials to model critical sized clusters, or use ab initio potentials to model very small clusters, the DNTEFP Monte Carlo method presented here can treat up to critical sized clusters using the effective fragment potential (EFP), a rigorous nonempirical intermolecular model potential based on ab initio electronic structure theory calculations, improvable in a systematic manner. The DNTEFP method is applied to study the evaporation rates, energetics, and structure factors of multicomponent clusters containing water and isoprene. The most probable topology of the transition state characterizing the evaporation of one water molecule from a water hexamer at 243 K is predicted to be a conformer that contains six hydrogen bonds, with a topology that corresponds to two water molecules stacked on top of a quadrangular $(H_2O)_4$ cluster. For the water hexamer in the presence of isoprene, an increase in the cluster size and a 3-fold increase in the evaporation rate are predicted relative to the reaction in which one water molecule evaporates from a water hexamer cluster.

Transition State Structure

TS Energy distribution
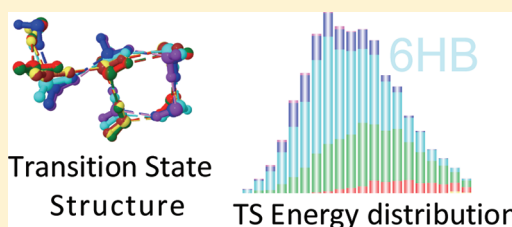
I. INTRODUCTION

Nucleation is an initial process that occurs in the formation of aerosols, synthesis of nanoparticles, crystal growth, dissolution of waste forms, and waste separation in nuclear technology. Water cluster kinetics, in particular, are essential for understanding the chemical and physical processes in the formation of atmospheric aerosols, steam corrosion of turbines, and formation of clathrates. Aerosols, the minute solid particles or liquid droplets in soot, oceanic haze, smog, sprays, and polluted air have both direct and indirect effects including changing the global climate.[1−4] For example, sufficiently large aerosol particles in the upper atmosphere scatter sunlight back into space, reducing the amount of solar radiation that reaches the lower atmosphere.[4] Reactive chemicals are emitted into the lower atmosphere from the burning of gasoline, fossil fuels, biomass, and biogenic sources at a rate that is faster than the rate of natural processes that remove the chemicals. A consequence is a change in the composition and reactivity of atmospheric aerosols.[1] Once they are released into the atmosphere, the reactive species (e.g., volatile organic compounds such as isoprene) undergo a series of photochemical reactions that are responsible for the production and destruction of climatologically important species such as ozone and carbon monoxide. Addressing the chemistry of atmospheric aerosols is important, as changes in the composition of atmospheric aerosols in one part of the world affects global climate conditions. Molecular scale models based on thermodynamic and kinetic parameters are needed in the climate models to accurately predict the role of the heterogeneous chemical components that are present in atmospheric nanoclusters that are important in the formation of atmospheric aerosols.

The intermolecular potential between the molecules is the driving force for nucleation and competes with the entropic contributions to the free energy of nucleation. While the widely used classical nucleation theory (CNT)[3−5] uses bulk properties such as surface tension and the equilibrium chemical potential to model nucleation, the dynamical nucleation theory (DNT) developed by Schenter, Kathmann, and Garrett[6−12] uses a molecular description of clusters and the molecular interaction potential. At the core of DNT is the evaluation of rates using Variational Transition State Theory (VTST).[13] In VTST, dynamic processes are characterized in terms of equilibrium statistical mechanical partition functions of the components of the reaction, namely, the reactants, transition states, and products.[14] An essential step in the process is the identification of the dividing surface that separates products and reactants. The best estimate of the rate constant is obtained by variationally optimizing the dividing surface that minimizes the reactive flux, thus providing a means to identify the most important configurations associated with the nucleation.[7] The most practical way to obtain the relevant statistical averages and partition functions is by using the Metropolis Monte Carlo method.[15,16]

The most accurate and consistent way to treat the intermolecular interactions would be to use well-correlated quantum chemical methods to evaluate the intermolecular potential and to use this potential in the molecular nucleation theory. However, reliable quantum mechanical methods that include electron correlation (e.g., many body perturbation theory and coupled cluster methods)[17−23] scale as N^5-N^7, where N is the number of atomic basis functions. Such high scaling limits the size of the molecular system that can be studied. An alternate and feasible approach would be to use efficient and reliable model potentials to describe intermolecular interactions.

The effective fragment potential (EFP) method is a predictive first-principles based model potential method in which all parameters that describe the molecular fragments are obtained from ab initio electronic structure calculations, thereby allowing for realistic modeling of condensed phase chemistry.[24−33] The intermolecular energy terms are Coulomb, polarization, exchange repulsion, dispersion, and charge transfer interactions.

This paper presents the implementation of the dynamical nucleation theory effective fragment potential (DNTEFP) model, to predict evaporation rate constants. The DNTEFP procedure employs Monte Carlo and VTST methods to compute relevant statistical mechanical averages and partition functions enabling an efficient approach for modeling nucleation kinetics, with the molecular interactions evaluated using the EFP model potential.

The organization of the paper is as follows. In Sections 2A and 2B brief reviews of dynamical nucleation theory and the effective fragment potential are presented. In Section 3, the implementation details of the DNTEFP model for evaluating evaporation rates using partition functions obtained via Monte Carlo simulations are described. In Section 4, the DNTEFP method is applied to water clusters and isoprene−water clusters, and results are presented for the simulations, including the evaporation rates, the distribution of the energies, the structure factors, and the hydrogen bonding topology of configurations relevant to evaporation. Section 5 presents concluding remarks.

2A. NUCLEATION MODEL AND THE DYNAMICAL NUCLEATION THEORY

The kinetics of nucleation is modeled as an evolution of cluster populations by the addition or loss of monomers.

$$N_i + N_1 \underset{\alpha_{i+1}}{\overset{\beta_i}{\rightleftarrows}} N_{i+1} \tag{1}$$

where N_i and N_{i+1} denote clusters with i and $i+1$ monomers, respectively; α_{i+1} is the rate constant for evaporation of a monomer from the N_{i+1} cluster; and β_i is the rate constant for condensation of a monomer into the N_i cluster.[6,7] The monomers are often considered to have a fixed geometry as in the current work. The clusters are assumed to be in thermal equilibrium (in general, cluster populations do not have to be in equilibrium). Sequential monomer addition, as described in eq 1, produces a reaction path linking the populations of clusters N_i of different sizes.

In this work, the DNT model is used to evaluate the evaporation rate constant. DNT is based on VTST in which dynamic processes are characterized in terms of equilibrium statistical mechanical partition functions.[7] A spherical dividing surface separates the reactants and products and is centered at the center of mass of the cluster N_i.[7,8] The Helmholtz free energy, A_i, of a cluster

can be determined from the cluster canonical ensemble partition function, Q_i, as

$$A_i(T,r) = -k_B T \ln Q_i(T,r) \tag{2}$$

where T is the temperature; r is the radius of the cluster (i.e., the radius of the spherical dividing surface in configuration space); and k_B is the Boltzmann constant.

Considering the phase space of i interacting, indistinguishable particles, the total partition function of the system can be evaluated as an integral over configuration space $\{\mathbf{r}^{(i)}\}$ constrained by the spherical dividing surface

$$Q_i(T,r) = \left(\frac{2\pi m k_B T}{h^2}\right)^{3i/2} \frac{1}{i!} \int dr^{(i)} \exp\left[-\frac{U_i(r^{(i)})}{k_B T}\right]$$

$$\times \prod_j^i \Theta(r - |\mathbf{R}_i - \mathbf{r}_j|) \tag{3}$$

where m is a monomer mass; $\mathbf{r}^{(i)} = \{\mathbf{r}_1, \mathbf{r}_2, ..., \mathbf{r}_j ..., \mathbf{r}_i\}$, is a point in configuration space that represents the center of mass coordinates $\mathbf{r}_i$ of all monomers; $U_i(r^{(i)})$ is the interaction potential of the system; $\mathbf{R}_i$ is the coordinate vector of the center of mass of the cluster; and h is Planck's constant. The Heaviside step function Θ effectively constrains the integration to the spherical volume centered on the center-of-mass of the cluster N_i. The interaction potential U_i is chosen to be zero for infinitely separated molecules so that A_i goes to the ideal gas limit (i.e., noninteracting molecules) as the volume increases. The volume enclosed by the spherical surface serves as a variational parameter that characterizes the dividing surface.

Dynamic nucleation theory predicts[7] the evaporation rate constant for cluster N_i to be

$$\alpha(T,r_{cut}) = -(2\pi m k_B T)^{-1/2} \frac{dA_i(T,r)}{dr}\bigg|_{r=r_{cut}} \tag{4}$$

where r_{cut} is the radius of the dividing surface corresponding to the minimal total reactive flux.

The total reactive flux is proportional to the derivative of the partition function of the cluster with respect to the cluster radius:[7] $-(d[N_i]/(dt)\propto(dQ_i(T,r))/(dr)$. Thus, computing the cluster partition function at various cluster radii r and taking its numerical derivative near r_{cut} would be sufficient to calculate the evaporation rate. Typically, the configurational sampling needed to compute $Q_i(T,r)$ involves the variation of all molecular configurations in all volumes (the so-called "r_{sim} methodology"). However, for any two spherical volumes of radii r_1 and r_2 with $r_1 < r_2$, the configuration integral $Q_i(T,r_2)$ will contain all the configurations present in the configuration integral of $Q_i(T,r_1)$. This allows one to reuse the configurations in the smaller volume and thus decrease the overall required sampling. Using this so-called "r_{config} sampling methodology", the sampling of the derivative of the partition function 3 with respect to the cluster radius is performed[11]

$$\frac{dQ_i(T,r)}{dr} = \left(\frac{2\pi m k_B T}{h^2}\right)^{3i/2} \frac{1}{i!} \int dr^{(i)} \exp\left[-\frac{U_i(r^{(i)})}{k_B T}\right]$$

$$\times \Sigma_k^i \delta(r' - |\mathbf{R}_i - \mathbf{r}_j|) \prod_j^i \Theta(r' - |\mathbf{R}_i - \mathbf{r}_j|) \tag{5}$$

13988

dx.doi.org/10.1021/jp207429r |J. Phys. Chem. A 2011, 115, 13987–13996

The derivative restricts one or more monomers to lie on the surface of the spherical volume via the delta function $\delta(r' - |\mathbf{R}_i - \mathbf{r}_j|)$. Therefore, at each sampling step the value of $(dQ(T,r))/(dr)|_{r=r_{conf}}$ is sampled, where r_{conf} is the configuration radius, that is, the distance from the cluster center of mass to the center of mass of the farthest monomer. Using eqs 2 and 4 the evaporation rate constant can be found according to

$$\alpha(T, r_{cut}) = -\left(\frac{k_B T}{2\pi m}\right)^{1/2} \frac{1}{Q_i(T, r_{cut})} \frac{dQ_i(T,r)}{dr}\bigg|_{r=r_{cut}} \quad (6)$$

with the partition function evaluated as $Q_i(T,r_{cut}) = -\int_0^{r_{cut}} [(dQ_i(T,r))/(dr)]dr$. Since r_{cut} is the value of r that corresponds to the minimum of $(dQ_i(T,r))/(dr)$, it also corresponds to the minimal reactive flux. Only the reactive flux dependence on the cluster radius r_{conf} is considered and is directly obtained in the simulations.

The evaporation rates are computed for clusters up to nuclei of critical size, characterized by a cluster radius beyond which condensation proceeds at a much faster rate than the rate of evaporation, and consequently the cluster grows rapidly from nanocluster size to macrocluster size. The equilibrium cluster distribution and condensation rate constants can then be estimated. In the present work, the molecular interaction potential is computed using the efficient EFP approach.

2B. ELECTRONIC STRUCTURE THEORY BASED MOLECULAR INTERACTION POTENTIAL: THE EFFECTIVE FRAGMENT POTENTIAL

The effective fragment potential (EFP) method is a first-principles-based model potential that incorporates the essential components of the intermolecular interactions.[24−33] The original EFP1 potential was designed specifically to describe aqueous interactions. The EFP2 potential has no empirically fitted parameters and is therefore completely general for describing intermolecular interactions between any types of molecular fragments. The EFP1 fragment—fragment interaction energy is

$$E = E^{Coul} + E^{Pol} + E^{Rem} \quad (7)$$

The first term represents the Coulomb part of the electrostatic interactions and is obtained using a distributed multipole expansion[34]

$$E^{Coul} = \sum_{a \in A} \sum_{b \in B} \left[\frac{q_a q_b}{R_{ab}} - \frac{q_a R_{ab} \mu_b}{R_{ab}^2} - \frac{q_b R_{ab} \mu_a}{R_{ab}^2} + \dots \right] \quad (8)$$

where q_a, q_b can be either an electronic or nuclear charge on the expansion points a and b; μ_a, μ_b represent the dipole moments on a and b; R_{ab} is the distance between a and b; and A and B represent the fragments. The K expansion points are the atom centers and bond midpoints (e.g., for water $K = 5$). Stone has shown that several expansion points are needed to adequately represent the charge distribution of the fragment.[34] In the EFP method, the Coulomb term is expanded through octopoles.

The second term, E^{Pol}, in eq 7 is a polarization (induction) term that is treated using a finite field dipole-induced dipole model in which the interaction is iterated to self-consistency. The polarization term is expressed as

$$E^{Pol} = -\frac{1}{2} \Sigma_i^{N_{Pol}} (\alpha_i F_i^{tot})(F_i^{tot} - F_i^\mu) \quad (9)$$

where N_{Pol} is the number of polarizable points that are located at the centroids of the localized molecular orbitals; α_i is the polarizability tensor at point i;

$$F_i^\mu = \sum_j F_i^{\mu_j} \quad (10)$$

is the field at point i from the induced dipoles in all of the other fragments; and $F_i^{\mu_j}$ is the field at point i from the induced dipole j. The total field at i, F_i^{tot}, is given by

$$F_i^{tot} = F_i^{efp} + F_i^\mu \quad (11)$$

where F_i^{efp} is the field at the polarizable point i due to the static multipoles in the other fragments.

The polarizability is expressed in terms of individual localized molecular orbital (LMO) polarizability tensors for each LMO in the molecule; for example, there are two bond LMOs and two lone pair LMOs in water.

The third EFP1 term, E^{Rem}, in eq 7 is a remainder term that accounts for all interactions that are not accounted for in the first two terms. The remainder term is fit to the total potential energy surface of the water dimer obtained with Hatree—Fock (HF) or density functional theory (DFT), after subtracting the Coloumb and polarization contributions. For EFP1/HF, the remainder term includes exchange repulsion and charge transfer. For EFP1/DFT, some short-range correlation is included as well. The remainder term is fitted to a sum over exponential functions centered on the fragment atom centers and center of mass. The EFP1 approach has been successfully applied to several problems that involve aqueous interactions.[24−30]

The EFP2 method has no empirically fitted parameters,[31−33] so an EFP2 potential can be generated from first principles for any molecular species. All EFP2 parameters are generated automatically by a single ab initio calculation. The EFP2 fragment—fragment interaction energy is described as a sum of five terms

$$E = E^{Coul} + E^{Pol} + E^{XR} + E^{CT} + E^{Disp} \quad (12)$$

The first and second terms in eq 12 are evaluated as described for the EFP1 method. The third term in eq 12, E^{XR}, represents the intermolecular exchange repulsion interaction energy and is expressed in terms of intermolecular overlap and kinetic energy integrals.[29] The fourth term, E^{CT}, is the charge transfer interaction energy term derived using a supermolecule approach considering the interactions between the occupied valence molecular orbitals on one fragment with the virtual orbitals of another fragment.[29] An approximate formula for the charge transfer interaction in the EFP method was derived and implemented using a second-order perturbation treatment of intermolecular interactions for a pair of molecules.[29] The charge transfer term is the computationally most expensive term in the EFP2 approach.

The last term in the EFP2 interaction energy (eq 12) is the fragment—fragment dispersion energy and can be expressed in terms of the familiar inverse R expansion

$$E^{Disp} = \Sigma_n C_n R^{-n} \quad (13)$$

The coefficients, C_n, may be derived from the (imaginary) frequency dependent polarizabilities. If one employs only dipole polarizabilities, the dispersion expansion is truncated at the leading term, with $n = 6$. In the current EFP2 implementation, an estimate is used for the $n = 8$ term, in addition to the explicitly derived $n = 6$ term. The EFP dispersion interaction is expressed as a sum of LMO—LMO interfragment interactions. The EFP

13989

dx.doi.org/10.1021/jp207429r |J. Phys. Chem. A 2011, 115, 13987–13996

method has been successfully applied to various molecular systems treating a broad range of intermolecular interactions, at a small fraction of the cost of correlated ab initio computations that produce comparable accuracy.[31,32,35−38]

3. DNTEFP: IMPLEMENTATION DETAILS

In the DNTEFP method, the DNT model uses the EFP2 potential for describing intermonomer interactions. For water, the DNT model also uses the EFP1/HF and EFP1/DFT potentials. In the initial cluster configuration in the DNTEFP method, the fragments are randomly placed so that the farthest monomer fragment is at a distance less than or equal to r_{max} from the center of mass of the cluster, where r_{max} is taken to be the maximum spherical cluster radius considered in the simulation. As a rigid monomer has 6 degrees of freedom (3 translational and 3 rotational degrees of freedom), a cluster of i rigid monomers has $6i$ degrees of freedom. If one uses a fixed center of mass coordinate system for the entire cluster of i rigid monomers, the number of degrees of freedom is reduced to $6i - 3$.

A Metropolis Monte Carlo approach is used for sampling the configuration integrals of eq 3. Using a Boltzmann weight of the fragment interaction potential, $\exp[-(U_i(r^i))/(k_BT)]$, it is ensured that the configurations with more negative fragment− fragment interaction energies are more probable. Configurations are sampled using the r_{config} methodology in which the volume is treated as a configurational property, and hence the computational requirements of the method scale for the homogeneous case as $O(r_{max}^{3i-3})$.[12,39] The monomers (EFP fragments) undergo translational and rotational motions and explore the constraining volume based on statistical mechanical fluctuations. The translation or rotation of an EFP fragment is nontrivial in the sense that all the expansion centers and the involved localized molecular orbitals (LMOs) need to undergo the same transformation. Rotation of fragments is considered via an axis and rotation angle chosen in a random manner. In the current implementation, the translational and rotational step lengths can be dynamically adjusted to maintain a sufficiently high acceptance ratio.

In large-scale Monte Carlo simulations using realistic potentials, the available wall-clock and CPU times for a Monte Carlo simulation are often less than the time required to perform the desired number of steps; also, the possibility for hardware failure must be taken into account. In the DNTEFP implementation, a restart capability is available to ensure that the Markov chain is uninterrupted. Both positions and orientations of the EFP fragments are stored regularly and restored upon restart, along with the accumulated statistical data. Special care has been given to the restart of the generation of random numbers, to avoid artificially shortening the random number generator (RNG) period and consequently negatively affecting the quality of the Monte Carlo simulations. It has been found that the quality of the simulations can be sensitive to correlation in the random number sequences.[40] Restarting the RNG from a "random" source, such as system time, would destroy the reproducibility of the results without ensuring the quality of the random sequence. The present implementation, therefore, saves the complete internal state of the RNG and restores it upon restart. Thus, the implementation ensures that the sequence of Markov chain steps after the interruption and restart is *exactly the same* as it would have been without the interruption.

The current implementation allows one to choose the interaction potential of the fragments to be the Dang−Chang potential,[41] EFP1/HF or EFP1/DFT for water clusters. For general molecular clusters, the DNTEFP method computes the intermolecular interaction potential using the efficient EFP2 approach that contains no empirically fitted parameters. Computing of an EFP2 potential is more time-consuming than that of an EFP1 potential.

The statistical distributions of clusters, generated by the MC simulations, are binned in several radial bins of equal size Δr, covering the entire radial distance of interest; a minimum radius of zero is used. The r_{config} method will produce a canonical partition function which is related to the integral over each bin, $\int_{r-\Delta r}^{r}(dQ(T,r'))/(dr')dr'$ where r is the upper end of the bin interval.[11,12] The central quantity needed for evaluation of the evaporation rate constant, that is, the derivative of the Helmholtz free energy with respect to the radius, is evaluated directly from the binned dQ_i values.[11,12] The region of minimum flux that defines the dividing surface is found, and the evaporation rate is predicted using eq 6. After sampling millions of configurations and converging the distributions, r_{cut}, and the evaporation rate constant, the radial distribution function, structure factors, energy distribution, number of hydrogen bonds, and the topology of the most probable conformation are determined. In addition, the most probable topology of the transition state along with the energy distribution and the number of hydrogen bonds in the transition states are obtained for a given temperature. It is well-known from the work of Truhlar and co-workers that while the conventional transition state is associated with a saddle point on the potential energy surface between the reactant and product regions the transition state that is addressed here corresponds to the region of minimal reactive flux that all reactive trajectories must cross.[42,43] However, some nonreactive trajectories may also be counted as reactive so that the simple transition state theory (TST) provides an upper bound to the exact reactive flux of classical trajectories through the dividing surface. The conventional transition state can thus be seen as a first approximation to the variationally optimized transition states. The above DNT model using the EFP potentials and Monte Carlo sampling for evaluating the configuration integrals is called the DNTEFP method and has been implemented in the GAMESS computational package.[44,45]

4. RESULTS FOR WATER CLUSTERS AND ISOPRENE− WATER CLUSTERS

Understanding the nucleation of pure water is an essential step toward the study of nucleation in more complex multicomponent systems. For example, in atmospheric chemistry, the role of contaminants in the nucleation of aerosols is crucial for understanding complex aerosol dynamics. Viewing the multistep kinetics of the nucleation process in terms of cluster growth controlled by monomer association and dissociation is quite reasonable as the average distance between the clusters is much larger (about 10^7 Å at 243 K and a 10-fold super saturation) than the average distance between water monomers (about 200 Å at these conditions). To show the efficacy of the DNTEFP approach, small water clusters are initially studied at 243 K since comparisons with previous results are possible.[11,12,35,46,47] In addition, isoprene clusters with water are studied to demonstrate the ability of this method to deal with multicomponent systems.

4A. DNTEFP Evaporation Rate Constants for Water Clusters. DNTEFP simulations of evaporation rate constants at 243 K were performed for water clusters using the EFP1/DFT and EFP2 interaction potentials. The EFP2 potential for water was

13990

dx.doi.org/10.1021/jp207429r |*J. Phys. Chem. A* 2011, 115, 13987−13996

Table 1. Evaporation Rate Constant and r_{cut} for Water Clusters at 243 K (DNTEFP Model)

	R_{cut} (Å) (DNTEFP model)		rate $\times$ 10^9 s^{-1} (DNTEFP model)		earlier work[48] (DNTDC model)	
$(H_2O)_n$ clusters	EFP2-CT	EFP2-noCT	EFP2-CT	EFP2-noCT	R_{cut}	rate $\times$ 10^9 s^{-1}
$n = 2$	2.64	3.14	46	51	2.8	160
$n = 3$	3.46	3.72	6.5	5.6	4.3	49
$n = 4$	4.34	4.56	0.34	1.6	5.8	4.7
$n = 5$	4.45	4.41	16	29	5.8	9.9
$n = 6$	4.73	4.79	48	32	6.3	13
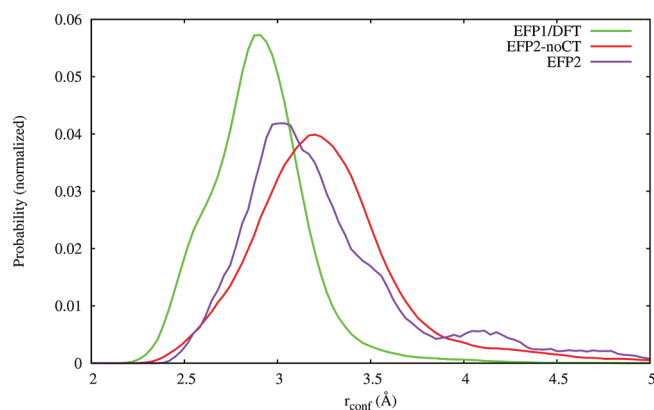
Figure 1. Distribution of cluster radius r_{config} of $(H_2O)_6$ using the EFP1/DFT, EFP2-noCT, and EFP2 potentials. The radius r_{config} refers to the radius of a spherical volume centered at the center of mass.

Figure 2. Oxygen–oxygen distance distribution of water hexamer at 243 K.

obtained at the equilibrium geometry with the 6-311++G (d, p)/HF level of theory.

The maximum radii considered in the simulations are 5.25, 6.75, 7.5, 7.5, and 7.75 Å for water dimer, trimer, tetramer, pentamer, and hexamer clusters, respectively. The maximum MC step sizes used for these studies are 0.04 Å for translational steps and 0.06 radians for rotational steps.

The evaporation rates predicted using the EFP2 potential with charge transfer (EFP2-CT) and without the charge transfer contribution (EFP2-noCT), respectively, are collected in Table 1. For comparison, the earlier Dang–Chang results are also shown in Table 1. Similar to earlier studies on water clusters using the Dang–Chang potential (DNTDC) the water tetramer cluster is predicted to be stable toward evaporation.[48]

4B. DNTEFP Statistical Parameters of Water Hexamer at 243 K. This section presents the statistical results for the water hexamer using the EFP potentials. To obtain the normalized values of the statistical parameters, the following approach is used. The statistical parameter (energy, angle, distance) range is divided into bins, and the number of hits of the parameter value in each of the bins is measured. The number of hits in each bin divided by the total number of hits in all the bins gives the normalized value for that parameter. Thus, the normalized value corresponding to each bin is the probability of the statistical parameter having a value within the range of that bin. If the size of the bin is sufficiently small, the normalized value divided by the bin size approximates the probability density. As all of the bins have the same size, the graph (the histogram) approximates the shape of the probability distribution.

The probability distribution of cluster radius r_{config} (the radius of the spherical cluster centered at the center of mass) for water
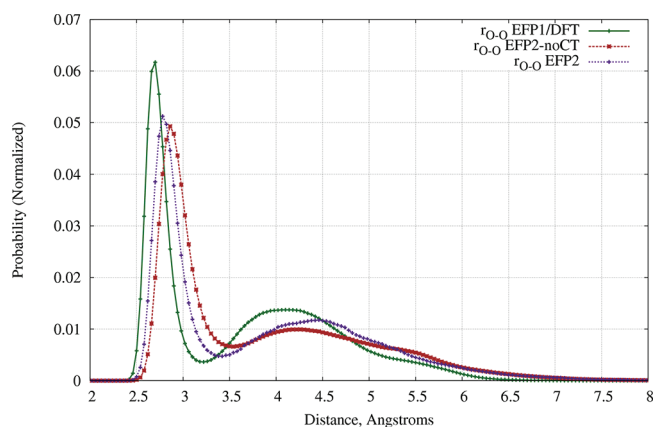
hexamer using three EFP potentials is presented in Figure 1 and provides a visual way to characterize the ensemble of the clusters. The r_{config} coordinate is plotted with values between 0 and 5.75 Å with a bin width of 0.03–4.5 Å. The distribution plot shows three distinct features: (1) a region of high probability around r_{config} = 3.0 Å corresponding to configurations where monomers are close together and interacting; (2) a region of low probability where r_{config} is between 3.5 and 4.5 Å corresponding to configurations where water monomers have a kinetic bottleneck as water monomers separate and where r_{cut} is determined; and (3) a region of slowly and monotonically increasing probability for r_{config} values greater than 4.5 Å corresponding to an entropic region where the interaction potential between monomers becomes flat and configurational spaces continue to increase in size. These three characteristic regions of the probability distribution are called the interaction, bottleneck, and entropic regions, respectively.

The DNTEFP computations for the EFP1/DFT potential used 16 million configurations and predict the radius that characterizes the dividing surface, r_{cut}, to be at 4.35 Å and the evaporation rate constant to be 270×10^9 s^{-1}. This rate constant is significantly higher than the rates predicted using EFP2 potentials (see Table 1) without and with the charge transfer term. The smaller r_{cut} predicted using the EFP1/DFT potential, compared with 6.3 Å for the Dang–Chang potential and 3.7–3.8 Å for EFP2, suggests that either the EFP method tends to overbind the clusters or Dang–Chang tends to underbind them, or both.

The oxygen–oxygen radial distribution was analyzed to understand the structure factors and is illustrated for the water hexamer in Figure 2. There is a significant peak in the probability of O–O distances at 2.85 Å corresponding to an O–O distance
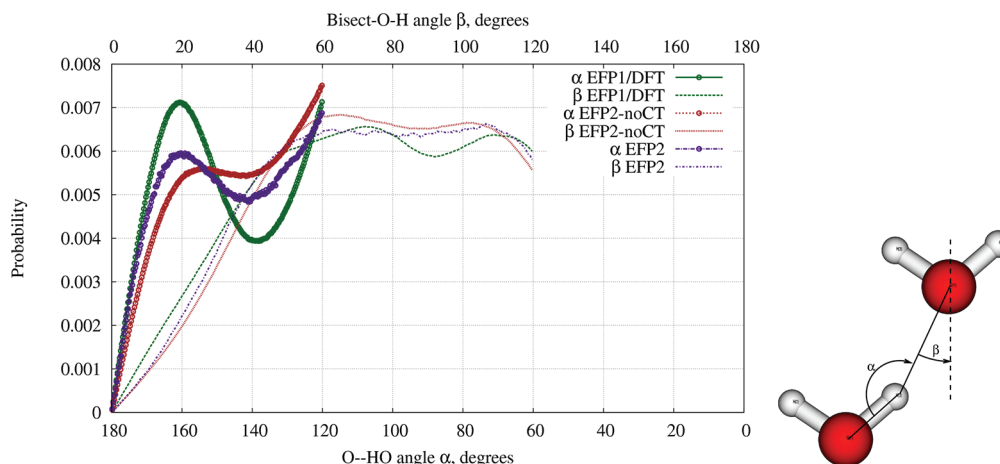
Figure 3. O—HO angle (α) and the bisector OH angle (β) distribution in $(H_2O)_6$ at 243 K.

consistent with hydrogen bonding.[39] The second broad peak at 3.5—5.5 Å is a signature of the first sphere of solvation as seen in the bulk.[49] This peak is attributed to the three-dimensional hydrogen bonded network. It is interesting that this feature is seen distinctly in water clusters as small as the hexamer.

Comparing the O—O distances predicted by the DNTEFP Monte Carlo simulations, it is seen that the O—O distances predicted by the EFP1/DFT and EFP2 potentials without and with the charge transfer term agree with each other within 0.2 Å. The same trend is seen for both the first sharp peak and the second broad peak. Inclusion of the charge transfer term in EFP2 shows little effect on the distribution and is consistent with observations from the cluster radius distribution that DFT tends to predict smaller sized clusters. As charge transfer is a short-range interaction, the effects on the Markov chain are significant only when the fragments are in close proximity.

To understand the relative orientations of the donor and the acceptor molecules with respect to the hydrogen bond, the OH—O angle and the OH bisector vector angle were analyzed graphically; the results for the water hexamer at 243 K are presented in Figure 3. The OH—O angle (α angle in Figure 3) defines the bend of a (near-linear) hydrogen bond, measured as the angle between the H—O bond of the donor molecule and the H—O vector from the hydrogen of the donor molecule to the oxygen of the acceptor molecule.

The bisector—OH angle (β angle in Figure 3) defines the orientation of the acceptor molecule with respect to the hydrogen bond and is measured as the angle between the main symmetry axis of the acceptor molecule and the vector from the acceptor oxygen to the hydrogen atom of the donor molecule. The probability distribution graphs were constructed with only those values of the angles that are reasonable for hydrogen-bonded molecules, namely, $180° \leq \alpha \leq 120°$ and $0° \leq \beta \leq 120°$. The distribution of the OH—O angles shows a distinct maximum around 165°, indicating that the majority of hydrogen bonds is slightly (up to 20°) bent. The maximum of the bisector—OH angular distribution is not so pronounced, with the plateau around 60—100 °, showing that the relative orientation of the donor molecule and the acceptor molecule with respect to the hydrogen bonds varies. To the best of our knowledge, these are the first angular distribution results showing the relative orientations of water molecules in the water hexamer cluster at 243 K.

To obtain the energy distribution of the conformers and topologies sampled in the calculations, the number of hydrogen
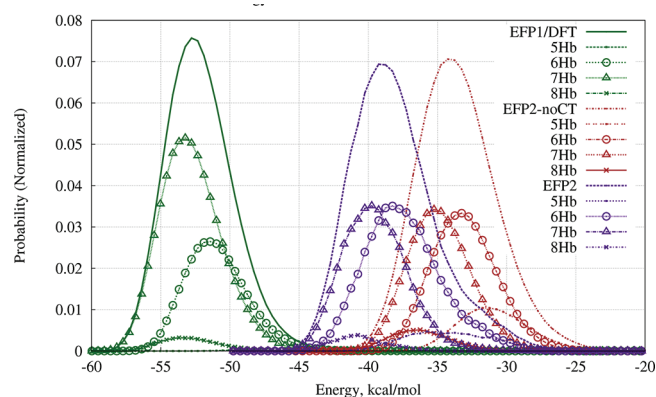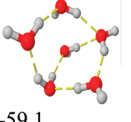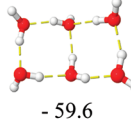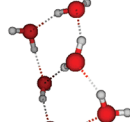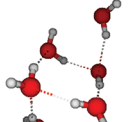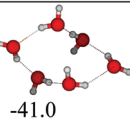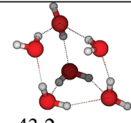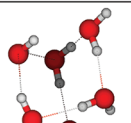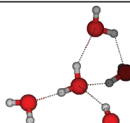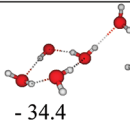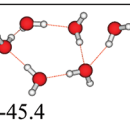

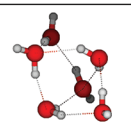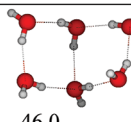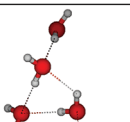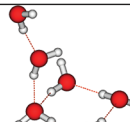**Figure 4.** Energy distribution of $(H_2O)_6$ at 243 K. The total distribution is given along with its decomposition into component distributions having between 5 and 8 hydrogen bonds (Hbs).

bonds (Hb's) in the sampled configurations has been evaluated and binned using a definition of a hydrogen bond with a characteristic hydrogen—oxygen distance between 1.4 and 2.5 Å.[36] As all of the bins have the same size, the graph (the histogram) approximates the shape of the probability distribution. The total energy distributions for the water hexamer at 243 K, as predicted by the DNTEFP Monte Carlo simulations using the EFP1/DFT, EFP2-noCT, and EFP2 potentials, are shown in Figure 4. The decomposition of the total distribution into component distributions that have between 0 and 8 hydrogen bonds (8Hb) was analyzed, and the relevant component distributions containing 5, 6, 7, and 8 hydrogen bonds (5Hb, 6Hb, 7Hb, and 8Hb) are also presented in Figure 4. Structures with less than 5 hydrogen bonds account for less than 5% of the distribution. The EFP1/DFT method predicts the hexamer to be more bound than do EFP2 and EFP2-noCT. Comparing the binding energies predicted using the EFP2-noCT and EFP2 methods, it is observed that the inclusion of the charge transfer interaction results in marginally greater binding energies. Analysis of the total energy distribution and the component energy distributions of conformers that have 5—8 hydrogen bonds illustrates that the maximum of the energy distribution (area under the curve) corresponds mostly to the conformers that contain 6 and 7 hydrogen bonds.

Table 2. Minimal and Most Probable Conformers of $(H_2O)_6$ at 243 K

DNTEFP Potentials	Energy (kcal/mol)				
	Minimal 6Hb	Minimal 8Hb	Minimal 7Hb	Most Probable 7Hb	Most Probable 6Hb
EFP1/DFT	-58.2	-59.1	- 59.6	-53.2	- 53.7
EFP2-noCT	-41.0	-43.2	-43.2	- 34.5	- 34.4
EFP2	-45.4	-45.8	-46.0	-39.1	-39.1

The DNTEFP predicted geometries of conformers of the water hexamer at 243 K, computed using the EFP1/DFT, EFP2-noCT, and EFP2 potentials, are binned according to the topologies containing 6, 7, and 8 hydrogen bonds; the minimum energy conformers are presented in Table 2. An analysis is carried out of the bins containing conformers with 6Hb and 7Hb to predict those 6Hb and 7Hb geometries that have the most probable energies. Energy bins are resolved to 0.5 kcal/mol, so the geometries are accurate to that interval. It is assumed that among the conformers containing the same number of hydrogen bonds the conformers with energy differences less than 0.5 kcal/mol have a similar topology. A check on a subset of the data shows this to be the case.

Geometries of the conformer with the minimal and most probable energy values for the 6, 7, and 8 hydrogen bonded conformers predicted using the three different EFP potentials for water hexamer at 243 K are presented in Table 2. Energy values reported are intermolecular interaction energies, and a zero value corresponds to the energy of infinitely separated monomers.

Table 2 shows the minimal and most probable hydrogen bonded structures that are relevant for water nucleation at 243 K. While the minimal energy structures with 6 and 7 hydrogen bonded conformers are book and prism like structures, the minimal energy 8 hydrogen bonded conformer predicted with three different potentials in DNT correspond to cage like structures. DNTEFP computations predict the geometries of the most probable 6 and 7 hydrogen bonded conformers to be the ones in which two water molecules are stacked together with a quadrangular water tetramer cluster. While the minimal energy structures reported are well-known prism, cage, and book topologies for water hexamer, the most probable topology reported here for the

water hexamer is a new structure (two water molecules stacked together with a quadrangular water tetramer cluster) and is identified as relevant to water nucleation at 243 K. The structures shown in Table 2 are consistent with the oxygen—oxygen distance and the angular distributions shown in Figures 2 and 3.

The DNTEFP method explores the region of minimum flux and the dividing surface region that separates the reactants and products. The conventional transition state can thus be seen as a first approximation to the variationally optimized transition state. In the r_{config} methodology, the bin corresponding to the dividing surface is obtained directly, thereby sampling the conformations of the transition states.

The transition state energy distribution (distribution of interaction energy values of water hexamers with a different number of hydrogen bonds in the bin corresponding to the critical radius, r_{cut}, of water hexamer at 243 K using the EFP2 potential, without and with the charge transfer term, along with the component distributions containing 3—8 hydrogen bonds) is represented as stacked histograms (each histogram bar is divided into sections whose heights indicated the proportion of observations falling into a given category, that is, the number of hydrogen bonds) which are shown in Figures 5 and 6, respectively. Structures containing 0—2 hydrogen bonds were not observed in the bin corresponding to the critical radius.

Analysis of the total energy distribution and the component energy distributions of conformers having 3—8 hydrogen bonds in Figures 5 and 6 illustrates that the maximum of the energy distribution corresponds to the conformers containing 6 hydrogen bonds (see the long light blue columns for 6Hb in Figures 5 and 6). The relative energy distribution is not strongly affected by the inclusion of the charge transfer term in the EFP2 calculations.
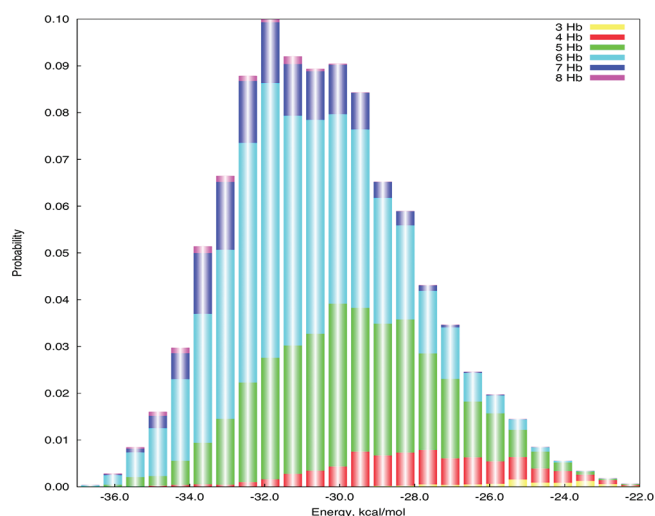
Figure 5. Transition state energy distribution for the evaporation reaction of $(H_2O)_6$ at 243 K using the EFP2 potential without the charge transfer term. The total distribution is given as a stacked histogram of component distributions having between 3 and 8 hydrogen bonds (Hbs).

Figure 6. Transition state energy distribution for evaporation reaction of $(H_2O)_6$ at 243 K using the EFP2 potential including the charge transfer term. The total distribution is given as a stacked histogram of component distributions having between 3 and 8 hydrogen bonds (Hbs).
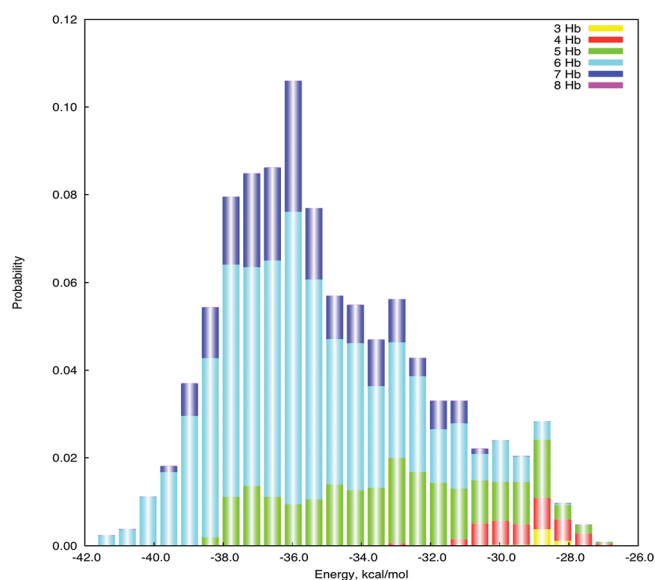
Analyzing the energy distribution of 6Hb conformers, the minimal energy transition state geometries using the EFP2-noCT and EFP2 potential were obtained and are presented in Figures 7 and 8, respectively. The low-lying 6Hb conformers in the bin corresponding to the transition state geometries were overlaid to arrive at the most probable topology of the transition state. The stacking tendency is seen in the minimal energy geometries predicted using DNTEFP2 without and with the charge transfer term.

The analysis of transition state energy distributions computed using the EFP2-noCT and EFP2 potentials suggests that the topology of the transition state predicted by both potentials is a 6H-bonded configuration in which four water molecules are arranged in a ring, with two additional water molecules perpendicular to the ring.

DNTEFP is based on VTST and concepts of classical statistical mechanics and does not account for nuclear quantum effects such as tunneling and zero point energy. Classical molecular dynamics (CMD) and path integral molecular dynamics (PIMD) simulations of water clusters using the classical TIP4P potential revealed that the inclusion of quantum effects leads to less structured clusters.[50,51] Recent ab initio PIMD simulations on water dimer at 50 K reveal that quantum nuclear effects result in ~15% weaker H bonds.[52] The use of empirical potentials with ZPE corrections and quantum statistical effects has been explored in the literature, where it was suggested that the effective potentials perform better than the classical potentials in the low-temperature region.[51]

4C. DNTEFP Evaporation Rate Constants for Multicomponent Isoprene−Water Clusters.

Volatile organic compounds (VOCs), present in the atmosphere, affect radiative forcing—a measure of how the energy balance between the amount of energy gained from incoming solar radiation flowing into the earth's atmosphere and the energy lost due to invisible infrared radiation from the earth's atmosphere back into space is altered: a positive balance leads to global warming, while a negative balance leads to cooling.[53] The boundary between the troposphere (the lowest level of the atmosphere) and the stratosphere (the very thin upper layer) is the region where the radiative forcing (energy imbalance) can be measured in a meaningful way. Isoprene, emitted by terrestrial vegetation, is the most abundant VOC in the atmosphere; hence it is important to understand the molecular origins of the effect of isoprene on the nucleation kinetics of water.[54]

The effect of isoprene on the nucleation rate of water was studied by computing the evaporation rate of a water hexamer cluster in the presence of a single isoprene molecule. Using the multicomponent formalism of DNT, a multicomponent DNTEFP method was implemented to compute the evaporation rate of molecular clusters.[55] The EFP2 potential for isoprene was obtained with RHF/6-311++G(d,p) using the NIST geometry.[56] The maximum of the cluster radius is taken to be 8.5 Å. The maximum MC step sizes used for these studies are 0.04 Å for translational steps and 0.06 radians for rotational steps. The DNTEFP computations of the evaporation rate of one water molecule from the water hexamer cluster in the presence of an isoprene molecule predict an increase in cluster size from 4.73 Å for the water hexamer to 5.4 Å. The increase in cluster size is expected, as the interaction between isoprene and water is aquaphobic. The DNTEFP computed evaporation rate constant for the evaporation of one water molecule from the isoprene−water cluster is predicted to be 105×10^9 s^{-1} and is three times the rate observed for the water hexamer (32×10^9 s^{-1}) at the same level of theory. The predicted evaporation rate increase for the water cluster in the presence of isoprene supports the experimental observations that suggest that nucleation is hindered by the presence of isoprene. A systematic and thorough investigation of the isoprene−water cluster nucleation kinetics will be the subject of future work. The preliminary computations presented here comprise an example to demonstrate the extended capability of the DNTEFP model to predict the reaction rates of multicomponent systems.
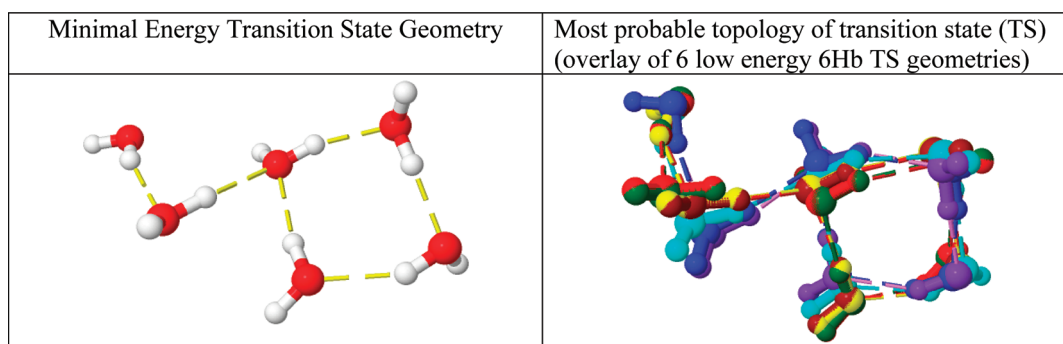
13994

dx.doi.org/10.1021/jp207429r |J. Phys. Chem. A 2011, 115, 13987–13996

Minimal Energy Transition State Geometry	Most probable topology of transition state (TS) (overlay of 6 low energy 6Hb TS geometries)

Figure 7. Minimal and most probable transition state geometries of $(H_2O)_6$: DNTEFP2-noCT.

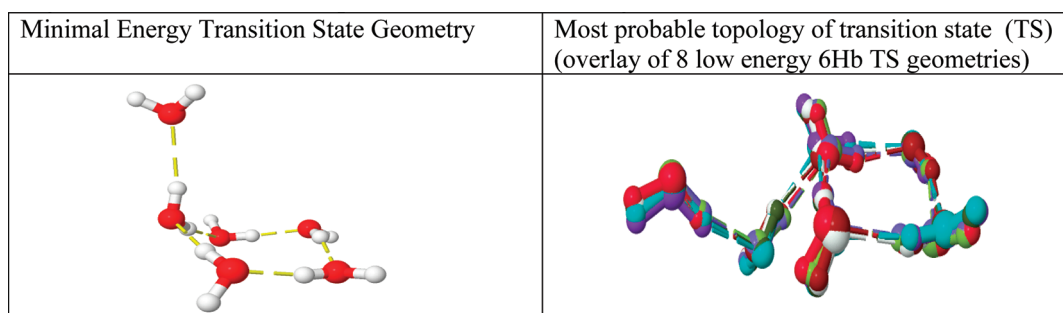| Minimal Energy Transition State Geometry	Most probable topology of transition state (TS) (overlay of 8 low energy 6Hb TS geometries)

Figure 8. Minimal and most probable transition state geometries of $(H_2O)_6$: DNTEFP2.

■ CONCLUSIONS

In this paper, the dynamical nucleation theory (DNT) model using the electronic structure theory based effective fragment potential (EFP2) method is implemented to evaluate the nucleation kinetics for multicomponent molecular clusters. On the basis of the variational transition state theory (VTST) method, the DNT model determines the region of minimum flux and the dividing surface characterizing the nucleation. The radius of the cluster that corresponds to a minimum in the reactive flux is obtained in a variational way, using metropolis Monte Carlo sampling of the configuration phase space spanned by the reactants, transition states, and the product states. The Monte Carlo simulations were performed using the r_{config} methodology that determines the change in the free energy of the cluster as a function of changing the volume in a direct way. For modeling nucleation kinetics of water clusters, the Dang—Chang, EFP1/HF, and EFP1/DFT potentials were also implemented.

The DNTEFP method was applied to water clusters, and the results confirm that the water tetramer cluster is stable toward evaporation. Statistical parameters of the DNTEFP method using different EFP potentials were analyzed for the water hexamer cluster at 243 K. Minimal energy geometries and the energy distribution of the most probable conformers sampled in the simulation were analyzed, and the methods predict the most probable conformers to be the ones with six and seven hydrogen bonds.

The variationally obtained radius of the dividing surface characterizes the transition states; hence the energy distribution in the bin corresponding to this radius was analyzed to find the most probable topology of the transition state characterizing the evaporation of water hexamer at 243 K.

The most probable transition state conformer is predicted to be a six hydrogen bonded topology in which two water molecules are stacked on top of a quadrangular water tetramer cluster. This apparently is the first time that the hydrogen bonded networks of the transition state ensemble corresponding to the evaporation reaction of water from a water cluster have been characterized using ab initio based potentials.

The DNTEFP method was applied to model the nucleation kinetics of a multicomponent system of water hexamer with isoprene—a climatologically essential biogenic emissive compound. The results suggest that the presence of isoprene increases the cluster size. The evaporation rate of a reaction in which a water molecule evaporates from the molecular cluster containing a water hexamer and isoprene is computed to be three times the rate computed for the reaction in which a water molecule evaporates from a water hexamer cluster. In a future paper, the development of a high-performance multichain, multilevel parallel DNTEFP Monte Carlo method using the general distributed data interface (GDDI)[57,58] to study water nucleation kinetics in the presence of ions will be discussed.

■ AUTHOR INFORMATION

Corresponding Author
*E-mail: mark@si.msg.chem.iastate.edu.

13995

dx.doi.org/10.1021/jp207429r |*J. Phys. Chem. A* 2011, 115, 13987–13996

national scientific user facility located at the Pacific Northwest National Laboratory (PNNL). PNNL is operated by Battelle for the U.S. Department of Energy.

■ REFERENCES

(1) Ziemann, P. J. Nature 2009, 46, 117.

(2) Andrese, M. O.; Rosenfeld, D. Earth. Sci. Rev. 2008, 89, 131.

(3) Seinfeld, J. H. Atmospheric Chemistry and Physics of Air pollution; Wiley: New York, 1986.

(4) Seinfeld, J. H.; Charlson, R.; Durkee, P. A.; Hegg, D.; Huebert, B. J.; Kiehl, J.; McCormick, M. P.; Ogren, J. A.; Penner, J. E.; Ramaswamy, V.; Slinn, W. G. N.; Slade, D. H.; Bouadjemi, D. Aerosol Radiative Forcing and Climate Change; National Academy Press: Washington, D.C., 1996.

(5) Abraham, F. F. Homogeneous Nucleation Theory; Academic Press: New York, 1974.

(6) Reiss, H. In 15th International Conference on Nucleation and Atmospheric Aerosols; Hale, B. N., Kulmala, M., Eds.; AIP, Conf. Proc., Rolla, Missouri, USA, American Institute of Physics: Melville, NY, 2000; Vol. 534, p 181.

(7) Shenter, G. K.; Kathmann, S. M.; Garrett, B. C. J. Chem.Phys. 1999, 110, 7951.

(8) Kathmann, S. M.; Schenter, G. K.; Garrett, B. C. J. Chem. Phys. 2002, 116, 5046.

(9) Kathmann, S. M.; Schenter, G. K.; Garrett, B. C. J. Chem. Phys. 2004, 120, 9133.

(10) Kathmann, S. M.; Schenter, G. K.; Garrett, B. C. Phys. Rev. Lett. 2007, 98, 109603.

(11) Crosby, L. D; Kathmann, S. M.; Windus, T. L. J. Comput. Chem. 2009, 30, 743.

(12) Windus, T. L.; Kathmann, S. M.; Crosby, D. L. J. Phys.: Conf. Ser. 2008, 125, 012017.

(13) Garret, B. C.; Truhlar, D. G. J. Phys. Chem. 1979, 83, 1052.

(14) Wigner, E. Trans. Faraday Soc. 1938, 34, 29.

(15) Metropolis, N.; Ulam, S. J. Am. Stat. Assoc. 1949, 44, 335.

(16) Metropolis, N.; Rosenbluth, A. W.; Rosenbluth, M. N.; Teller, A. H.; Teller, E. J. Chem. Phys. 1953, 21, 1087.

(17) Schmidt, M. W.; Gordon, M. S. Annu. Rev. Phys. Chem. 1998, 49, 233.

(18) Windus, T.L.; Schmidt, M.W.; , Gordon, M.S. Parallel Processing With the Ab Initio Program GAMESS. In Toward Teraflop Computing and New Grand Challenge Applications; Kalia, R. J., Vashishta, P., Eds.; Nova Science Publishers: New York, 1995; Vol. 9, p 189.

(19) Ajitha, D.; Pal, S. J. Chem. Phys. 2001, 114, 3830.

(20) Ajitha, D.; Fedorov, D. G.; Finley, J. P.; Hirao, K. J. Chem. Phys. 2002, 117, 7068.

(21) Devarajan, A.; Gaenko, A. V.; Khait, Y. G.; Hoffmann, M. R. J. Phys. Chem A 2008, 112, 2677.

(22) Devarajan, A.; Gaenko, A.; Lindh, R.; Malmqvist, P.Å. Int. J. Quantum Chem. 2009, 109, 1962.

(23) Devarajan, A.; Gaenko, A.; Autschbach, J. J. Chem. Phys. 2009, 130, 194102.

(24) Day, P. N.; Jensen, J. H.; Gordon, M. S.; Webb, S. P.; Stevens, W. J.; Krauss, M.; Garmer, D.; Basch, H.; Cohen, D. J. Chem. Phys. 1996, 105, 1968.

(25) Jensen, J. H.; Gordon, M. S. J. Chem. Phys. 1998, 108, 4772.

(26) Jensen, J. H. J. Chem. Phys. 2001, 114, 8775.

(27) Gordon, M. S.; Freitag, M. A.; Bandyopadhyay, P.; Jensen, J. H.; Kairys, V.; Stevens, W. J. J. Phys. Chem. A 2001, 105, 293.

(28) Adamovic, I.; Gordon, M. S. Mol. Phys. 2005, 103, 379.

(29) Li, H.; Gordon, M. S.; Jensen, J. H. J. Chem. Phys. 2006, 124, 214108.

(30) Adamovic, I.; Freitag, M. A.; Gordon, M. S. J. Chem. Phys. 2003, 118, 6725.

(31) Slipchenko, L. V.; Gordon, M. S. J. Comput. Chem. 2007, 28, 276.

(32) Slipchenko, L. V.; Gordon, M. S. Mol. Phys. 2009, 107, 999.

(33) Kemp, D. D.; Rintelman, J.; Gordon, M. S.; Jensen, J. H. Theor. Chem. Acc. 2010, 125, 481.

(34) Stone, A. J. Chem. Phys. Lett. 1981, 83, 233.

(35) Adamovic, I.; Li, H.; Lamm, M. H.; Gordon, M. S. J. Phys. Chem. A 2006, 110, 519.

(36) Smith, T.; Slipchenko, L. V.; Gordon, M. S. J. Phys. Chem. A 2008, 112, 5286.

(37) Slipchenko, L. V.; Gordon, M. S. J. Phys. Chem A 2009, 113, 2092.

(38) Mullin, J. M.; Roskop, L. B.; Pruitt, S. R.; Collins, M. A.; Gordon, M. S. J. Phys. Chem. A 2009, 113, 9945.

(39) Crosby, L. D.; Windus, T. L. J. Phys. Chem. A 2009, 113, 607.

(40) Vattulainen, I.; Kankaala, K.; Saarinen, J.; Ala-Nissila, T. Comput. Phys. Commun. 1995, 86, 209.

(41) Dang, L. X.; Chang, T. M. J. Chem. Phys. 1997, 106, 8149.

(42) Truhlar, D. G.; Isaacson, A. D.; Garrett, B. C. In Theory of Chemical Reaction Dynamics; Baer, M., Ed.; CRC: Boca Raton, FL, 1985; Vol. IV, p 65.

(43) Truhlar, D. G.; Garrett, B. C.; Klippenstein, S. J. J. Phys. Chem. 1996, 100, 12771.

(44) Schmidt, M. W.; Baldridge, K. K.; Boatz, J. A.; Elbert, S. T.; Gordon, M. S.; Jensen, J. J.; Koseki, S.; Matsunaga, N.; Nguyen, K. A.; Su, S.; Windus, T. L.; Dupuis, M.; Montgomery, J. A. J. Comput. Chem. 1993, 14, 1347.

(45) Gordon, M. S.; Schmidt, M. W. In Theory and Applications of Computational Chemistry, The First Forty Years; Dykstra, C. E., Frenking, G., Kim, K. S., Scuseria, G. E., Eds.; Elsevier: Amsterdam, 2005; pp 1167−1189.

(46) ten Wolde, P. R.; Ruiz-Montero, M. J.; Frenkel, D. J. Chem. Phys. 1999, 110, 1591.

(47) Schaaf, P.; Senger, B.; Voegel, J. C.; Bowles, R. K.; Reiss, H. J. Chem. Phys. 2001, 114, 8091.

(48) Kathmann, S. M.; Palmer, B. J.; Schenter, G. K.; Garrett, B. C. J. Chem. Phys. 2008, 128, 64306.

(49) Netzloff, H. M.; Gordon, M. S. J.Chem. Phys. 2004, 121, 2711.

(50) Schenter, G. K. J. Chem. Phys. 2002, 117, 6573.

(51) Hodges, M. P.; Wheatley, R. J.; Schenter, G. K.; Harvey, A. H. J. Chem. Phys. 2004, 120, 710.

(52) Walker, B.; Michaelides, A. J. Chem. Phys. 2010, 133, 174306.

(53) Lenton, T. M.; Vaughan, N. E. Atmos. Chem. Phys. Discuss. 2009, 9, 2559.

(54) Kiendler-Scharr, A.; Wildt, J; Maso, M. D.; Hohaus, T.; Kleist, E.; Mentel, T. F.; Tillmann, R.; Uerlings, R.; Schurr, U.; Wahner, A. Nature 2009, 461, 381.

(55) Kathmann, S.; Schenter, G. K.; Garret, B. C. J. Chem. Phys. 2004, 120, 9133.

(56) http://webbook.nist.gov/ (accessed July 1, 2010).

(57) Schmidt, M. W.; Fletcher, G. D.; Bode, B. M.; Gordon, M. S. The Distributed Data Interface in GAMESS. Comput. Phys. Commun. 2000, 128, 190.

(58) Fedorov, D. G.; Olson, R. M.; Kitaura, K.; Gordon, M. S.; Koseki, S. A new hierarchical parallelization scheme: Generalized distributed data interface (GDDI), and an application to the fragment molecular orbital method (FMO). J. Comput. Chem. 2004, 25, 872.